J|A|C|S ARTICLES

Published on Web 09/10/2010

A Unifying Model for the Operation of Light-Emitting Electrochemical Cells

Stephan van Reenen,[†] Piotr Matyba,[‡] Andrzej Dzwilewski,[†] René A. J. Janssen,[†] Ludvig Edman,[‡] and Martijn Kemerink*,[†]

Department of Applied Physics, Eindhoven University of Technology, PO Box 513, 5600 MB Eindhoven, The Netherlands, and The Organic Photonics and Electronics Group, Department of Physics, Umeå University, SE-901 87 Umeå, Sweden

Received May 26, 2010; E-mail: m.kemerink@tue.nl

Abstract: The application of doping in semiconductors plays a major role in the high performances achieved to date in inorganic devices. In contrast, doping has yet to make such an impact in organic electronics. One organic device that does make extensive use of doping is the light-emitting electrochemical cell (LEC), where the presence of mobile ions enables dynamic doping, which enhances carrier injection and facilitates relatively large current densities. The mechanism and effects of doping in LECs are, however, still far from being fully understood, as evidenced by the existence of two competing models that seem physically distinct: the electrochemical doping model and the electrodynamic model. Both models are supported by experimental data and numerical modeling. Here, we show that these models are essentially limits of one master model, separated by different rates of carrier injection. For ohmic nonlimited injection, a dynamic p−n junction is formed, which is absent in injection-limited devices. This unification is demonstrated by both numerical calculations and measured surface potentials as well as light emission and doping profiles in operational devices. An analytical analysis yields an upper limit for the ratio of drift and diffusion currents, having major consequences on the maximum current density through this type of device.

Introduction

Light-emitting electrochemical cells (LECs) form an attractive alternative to the organic light-emitting diode (OLED). LECs differ from OLEDs by the presence of mobile ions in the active layer, resulting in a relative insensitivity of the device functionality to active layer thickness and electrode material,[1−7] which in turn opens the opportunity to fabricate devices comprising solely organic materials[8,9] by low-cost methods such as printing.[9,10] However, 15 years after the invention of LECs by Pei et al.,[11] the underlying device physics is still far from fully understood. Measurements have been interpreted in either of two models: the electrodynamic model (ED)[12−16] and the electrochemical doping model (ECD).[17−22] These models are best distinguished by regarding the predicted steady-state operation of LECs as shown in Figure 1. The former states that nearly all applied potential drops at two sheets of accumulated and uncompensated ions positioned in close proximity to the electrode interfaces (see Figure 1a). Next to the enhancement of carrier injection, these electric double layers (EDLs) screen the bulk polymer from the external electric field, resulting in a diffusion-dominated electronic current in the bulk. The electronic carriers in the bulk are electrostatically compensated by a difference between the anion and cation concentrations to prevent the formation of net space charge.[12] The ECD predicts EDL formation as well, but only as much of the applied potential

[†] Eindhoven University of Technology.
[‡] Umeå University.

(1) Leger, J. M. *Adv. Mater.* **2008**, *20*, 837–841.
(2) Sun, Q. J.; Li, Y. F.; Pei, Q. B. *J. Disp. Technol.* **2007**, *3*, 211–224.
(3) Edman, L. *Electrochim. Acta* **2005**, *50*, 3878–3885.
(4) Bolink, H. J.; Cappelli, L.; Coronado, E.; Grätzel, M.; Ortí, E.; Costa, R. D.; Viruela, P. M.; Nazeeruddin, Md. K. *J. Am. Chem. Soc.* **2006**, *128*, 14786–14787.
(5) Slinker, J. D.; Rivnay, J.; Moskowitz, J. S.; Parker, J. B.; Bernhard, S.; Abruña, H. D.; Malliaras, G. G. *J. Mater. Chem.* **2007**, *17*, 2976–2988.
(6) Buda, M.; Kalyuzhny, G.; Bard, A. J. *J. Am. Chem. Soc.* **2002**, *124*, 6090–6098.
(7) Marcilla, R.; Mecerreyes, D.; Winroth, G.; Brovelli, S.; Del Mar Rodriguez Yebra, M.; Cacialli, F. *Appl. Phys. Lett.* **2010**, *96*, 043308.
(8) Yu, Z.; Hu, L.; Liu, Z.; Sun, M.; Wang, M.; Grüner, G.; Pei, Q. B. *Appl. Phys. Lett.* **2009**, *95*, 203304.
(9) Matyba, P.; Yamaguchi, H.; Eda, G.; Chhowalla, M.; Edman, L.; Robinson, N. D. *ACS Nano* **2010**, *4*, 637–642.
(10) Mauthner, G.; Landfester, K.; Köck, A.; Brückl, H.; Kast, M.; Stepper, C.; List, E. J. W. *Org. Electron.* **2008**, *9*, 164–170.
(11) Pei, Q. B.; Yu, G.; Zhang, C.; Yang, Y.; Heeger, A. J. *Science* **1995**, *269*, 1086–1088.
(12) deMello, J. C.; Tessler, N.; Graham, S. C.; Friend, R. H. *Phys. Rev. B* **1998**, *57*, 12951–12963.
(13) deMello, J. C.; Halls, J. J. M.; Tessler, N.; Graham, S. C.; Friend, R. H. *Phys. Rev. Lett.* **2000**, *85*, 421–424.
(14) deMello, J. C. *Phys. Rev. B* **2002**, *66*, 235210.
(15) Slinker, J. D.; DeFranco, J. A.; Jaquith, M. J.; Silveira, W. R.; Zhong, Y.-W.; Moran-Mirabal, J. M.; Craighead, H. G.; Abrũa, H. D.; Marohn, J. A.; Malliaras, G. G. *Nat. Mater.* **2007**, *6*, 894–899.
(16) Malliaras, G. G.; Slinker, J. D.; DeFranco, J. A.; Jaquith, M. J.; Silveira, W. R.; Zhong, Y.-W.; Moran-Mirabal, J. M.; Craighead, H. G.; Abrũa, H. D.; Marohn, J. A. *Nat. Mater.* **2008**, *7*, 168.
(17) Hoven, C. V.; Wang, H.; Elbing, M.; Garner, L.; Winkelhaus, D.; Bazan, G. C. *Nat. Mater.* **2009**, *9*, 249–252.
(18) Matyba, P.; Maturova, K.; Kemerink, M.; Robinson, N. D.; Edman, L. *Nat. Mater.* **2009**, *8*, 672–676.
(19) Gao, J.; Dane, J. *Appl. Phys. Lett.* **2004**, *84*, 2778–2780.
(20) Pei, Q. B.; Heeger, A. J. *Nat. Mater.* **2008**, *7*, 168.
(21) Smith, D. L. *J. Appl. Phys.* **1997**, *81*, 2869–2880.
(22) Dick, D. J.; Heeger, A. J.; Yang, Y.; Pei, Q. B. *Adv. Mater.* **1996**, *8*, 985–987.

 10.1021/ja1045555

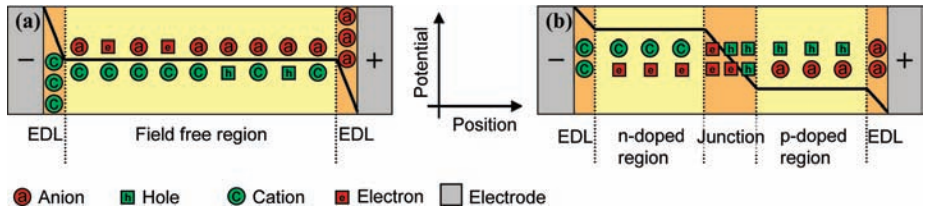

Figure 1. Schematic diagrams illustrating the potential profile and the electronic and ionic charge distribution in an LEC during steady-state operation. Potential profiles and charge distributions as predicted by (a), the ED and (b), the ECD. The thick black line represents the potential profile (in eV), and the electronic and ionic charge distributions are illustrated by the red (negatively charged) and green (positively charged) symbols, respectively. Furthermore, the high- and low-field regions in the bulk are accentuated by orange and light yellow, respectively. In the low-field regions, charges are mutually compensated, e.g. cations by anions or cations by electrons.

is dissipated at the EDLs as is needed to form ohmic contacts (see Figure 1b). The buildup of bulk space charge by the enhanced injection of electronic charge carriers is minimized by the response of the anions and cations. Anions (cations) move away from the electron (hole)-injecting contact. Hence, regions are formed in which electrons (holes) are electrostatically compensated by cations (anions). Because of the similarity to the (static) situation encountered in doped inorganic semiconductors, this process is commonly referred to as (electrochemical) doping of the conjugated polymer: in both cases a (relatively) immobile ionic species forms a neutral complex with an electronic charge. Since the amount of ions is limited and the amount of injected electrons and holes is not, anions and cations eventually become completely separated.[21] In between the p- and n-type regions, a narrow intrinsic region arises where the remainder of the applied potential drops and where electron−hole recombination takes place: a light-emitting p−n junction is formed. Also in the ED model 'partial' doping occurs, in the sense that the electronic charges on both sides of the recombination zone are compensated by (a difference in the concentration of) anions and cations.

Both models are supported by experimental data. Regarding the electrostatic potential, results have been obtained favoring either of the two models.[15,18,23] Electrochemical doping has been mainly advocated in support of the ECD and has been visualized in planar LECs under UV illumination by monitoring the doping-induced quenching of photoluminescence (PL).[19,24] Also, modeling studies favoring the ED[12−15] as well as the ECD[21,25,26] have appeared. It is clear that the inability of the current models in vogue to explain all experimental and numerical data impedes the further development of LECs.

Here, we present a unified description of LECs. Both the ED and the ECD are shown to be limiting situations of this master model, distinguished by the injection rate at the contacts. The numerical modeling results are confirmed by dedicated experiments and rationalize previous observations. An analytical evaluation of the steady-state situation shows that in the doped regions of LECs the electric field-driven drift current cannot exceed the diffusion current, which constrains the maximum device current.

Experimental Section

For the fabrication of devices, one of the following two conjugated polymers was used: poly[2-methoxy-5-(3′,7′-dimethyloctyloxy)-*p*-phenylenevinylene] (MDMO-PPV, $M_w > 1 \times 10^6$ g mol^{-1}, American Dye Source) or phenyl-substituted poly(*p*-phenylene vinylene) copolymer (SY-PPV, Merck, catalogue number PDY-132); the latter is commonly termed "superyellow". Poly(ethylene oxide) (PEO, $M_w = 5 \times 10^5$ g mol^{-1}, Aldrich) was used as received, and the salt potassium trifluoromethanesulfonate (KCF_3SO_3, 98%, Aldrich) was dried at 473 K under vacuum before use. The conjugated polymer (CP) SY-PPV was dissolved in cyclohexanone (>99%, anhydrous, Aldrich) at a concentration of 5 mg/mL, and the CP MDMO-PPV was dissolved in chloroform (>99.8%, anhydrous, Aldrich) at a concentration of 10 mg/mL. PEO and KCF_3SO_3 were dissolved separately in cyclohexanone (>99%, anhydrous, Aldrich) at 10 mg/mL concentration. These solutions were mixed together in a mass ratio of CP/PEO/KCF_3SO_3 = 1:1.35:0.25. This blend solution was thereafter stirred on a magnetic hot plate at a temperature $T = 323$ K for 5 h. Glass substrates (1×1 cm^2) were cleaned by subsequent ultrasonic treatment in detergent, distilled water, acetone, and isopropanol.

The glass substrates were spin-coated with the blend solution (at 800 rpm for 60 s, followed by 1000 rpm for 10 s) after which they were dried at $T = 323$ K for at least 1 h on a hot plate. The thickness of the active material film was ∼230 nm, as determined by profilometry. For the noninjection-limited devices, Au electrodes capped with a layer of Al were deposited by thermal evaporation under high vacuum ($p \approx 1 \times 10^{-6}$ mbar) on top of the spin-coated films. For injection-limited devices, purposely oxidized Al electrodes were utilized instead. The oxidation procedure consisted of preparing the spin-coated films in a glovebox under N_2 atmosphere in the presence of a small amount of oxygen ($[O_2] \approx 20$ ppm) before evaporation of Al, and the subsequent storage of the devices for ∼5 days before testing to allow the formation of an AlO_x injection barrier. A thin wire-based shadow mask was used to create an interelectrode gap of approximately 100 μm. All of the above-mentioned procedures, save for the cleaning of the substrates and the oxidation of the Al electrodes, were done in a glovebox under N_2 atmosphere ($[O_2] < 1$ ppm and $[H_2O] < 1$ ppm) or in an integrated thermal evaporator.

SKPM images were recorded in a glovebox under N_2 atmosphere ($[O_2] < 1$ ppm and $[H_2O] < 1$ ppm) with a Veeco Instruments MultiMode AFM with Nanoscope IV controller, operating in lift mode with a lift height of 25 nm. Ti−Pt-coated silicon tips (MikroMasch NSC36/Ti−Pt, $k \approx 1.75$ N m^{1-}) were employed. All measurements were carried out at $T = 333$ K.

Optical probing was performed in an optical-access cryostat under high vacuum ($p < 10^{-5}$ mbar), using a single-lens reflex camera (Canon EOS50) equipped with a macro lens (focal length: 65 mm) and a teleconverter (× 2). In parallel with the optical probing, the current was measured with a computer-controlled source-measure unit (Keithley 2612). The electrooptical probing was carried out at $T = 333$ K.

For the numerical simulations, a one-dimensional model was used, in which the active layer of length $L = 350$ nm was divided in $N = 81$ discrete, equidistant points. The numerical model solves the drift−diffusion equations for electrons, holes, anions, and cations and Poisson's equation on this grid by forward integration in time.

(23) Pingree, L. S. C.; Rodovsky, D. B.; Coffey, D. C.; Bartholomew, G. P.; Ginger, D. S. *J. Am. Chem. Soc.* **2007**, *129*, 15903–15910.
(24) Shin, J. H.; Edman, L. *J. Am. Chem. Soc.* **2006**, *128*, 15568–15569.
(25) Manzanares, J. A.; Reiss, H.; Heeger, A. J. *J. Phys. Chem. B* **1998**, *102*, 4327–4336.
(26) Riess, I.; Cahen, D. *J. Appl. Phys.* **1997**, *82*, 3147–3151.

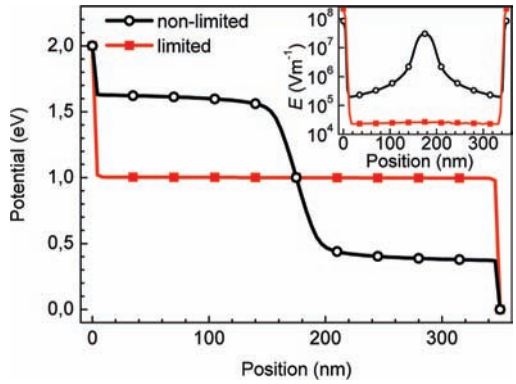

Figure 2. Simulation results for the potential profile in an LEC in steady state. The electrostatic potential profile $V(x)$ of the device that has (no) injection limitation corresponds to the red (black) line with squares (circles). The corresponding electric field $E = -dV/dx$ is shown in the inset.

Devices with a bandgap $E_g = 1$ eV were simulated during operation at a bias voltage $V_{bias} = 2$ V until steady state had been reached, recognized by a zero ion current. Initially, ions were homogeneously distributed at a density of 1.25×10^{25} m^{-3} as used by deMello.[14] No binding energy was assumed between anions and cations. The electrodes were ionically blocking and electrons and holes were injected from the contacts by use of different injection models, e.g. Fowler−Nordheim tunneling or Emtage O'Dwyer. The main difference between the various models is the resulting charge injection rate and its dependence on electric field, see Supporting Information. The injection barriers were set at 0.5 eV for both electrons and holes to simulate a symmetric device. Bimolecular electron−hole recombination was described by a Langevin process, and the electrostatic potential was determined by Poisson's equation. Furthermore, energetic and spatial disorder, as is present in real polymers, were omitted for convenience, as were charge traps. The following additional parameters were used: The relative dielectric constant $\varepsilon = 3$, $T = 300$ K, the electron and hole mobility $\mu_{p/n} = 10^{-6}$ m^2 V^{-1} s^{-1}. A relatively high anion and cation mobility could be chosen (10^{-7} m^2 V^{-1} s^{-1}) to speed up convergence since this parameter does not affect the outcome at steady state. It was checked that neither the magnitude of E_g and V_{bias} nor the thickness of the active layer affects the outcome of the calculations in a nontrivial manner, as long as $V_{bias} > E_g$ (see Supporting Information).

Results and Discussion

Simulations were done for different injection models (see Experimental Section), effectively altering the carrier injection rate. Consequently, the steady-state current of one device is limited by the injection process, whereas the other device is allowed to form a nonlimiting ohmic contact. In the latter case the current is limited by the bulk resistivity. Figure 2 shows the resulting potential profiles. In the noninjection-limited case, two EDLs have formed near the electrodes, dissipating as much potential as needed to overcome the injection barriers of 0.5 eV. The rest of the potential is dropped over a p−n junction formed in the bulk, in agreement with the ECD. In contrast, when injection is limited, two large EDLs are formed, dissipating nearly all applied potential in accordance with the ED. The electric field profiles shown in the inset clearly indicate that the electric field in the bulk is strongly reduced in the injection-limited case as compared to that of the nonlimited device.

The carrier distributions from both simulations at steady state are shown in Figure 3. In the nonlimited device (Figure 3a) the dopant anions and cations have been spatially separated, either for EDL formation or for doping of the polymer, i.e. for electrostatically compensating injected charge carriers. Due to

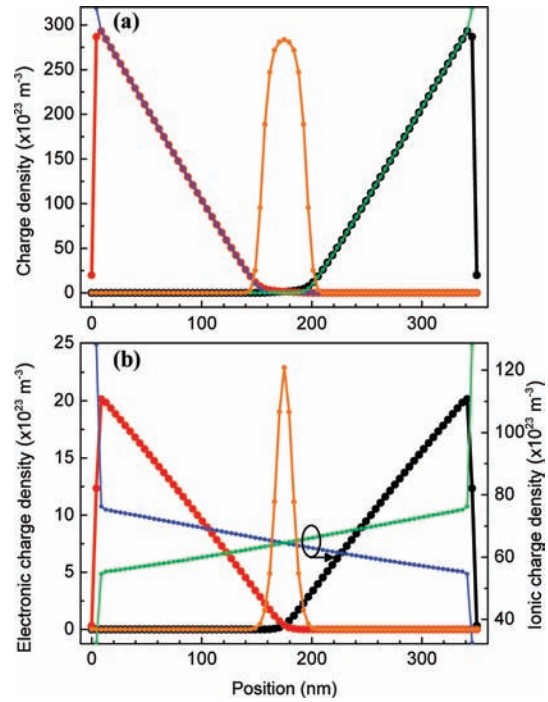

Figure 3. Simulation results for electronic and ionic charge carriers and recombination distributions in an LEC. Electron, hole, anion and cation densities are the red, black, green and blue lines, respectively. The orange line represents the recombination profile. No vertical axis is shown corresponding to the latter. The distribution profiles for an LEC in (a) the noninjection-limited regime and (b) the injection-limited regime are shown.

the symmetry of the simulated device the p−n junction is centered. In the central intrinsic region the charge of the electrons and holes is not compensated due to the absence of dopant ions. Hence, their space charge causes the potential drop observed in this region. This sets organic LECs apart from inorganic p−n junctions in which the space charge results from the ionized dopants.[21] The resulting large electric field compensates for the low conductivity in this region, so a constant current density is maintained throughout the device. In contrast, in the injection-limited device (Figure 3b) the dopant anions and cations are not fully spatially separated. Still, the ions are used to form EDLs as well as to do some minor doping. However, the doping is much less prominent due to the relatively low concentration of injected charge carriers. Consequently, a large fraction of ions remains paired to their counterions, instead of to an electron or hole, as in the noninjection-limited case. The (ionic and total) conductivity is therefore roughly constant throughout the device, and no distinct raise of the electric field in the recombination zone is necessary to warrant a constant current density throughout the device. Hence, no p−n junction is formed.

The calculated integrated recombination rate of the modeled LECs (see Figure 3) at steady state is approximately one decade larger in the ohmic regime than in the injection-limited regime. This difference is strongly dependent on the degree of injection limitation and may therefore become even more significant when injection becomes more problematic.

One characteristic that distinguishes LECs from other light-emitting devices like organic and inorganic LEDs with fixed doping is that upon reversing the polarity of the applied potential the device still functions the same: the mobile ions redistribute so that n- and p-doped regions exchange positions.[11,18,19] The

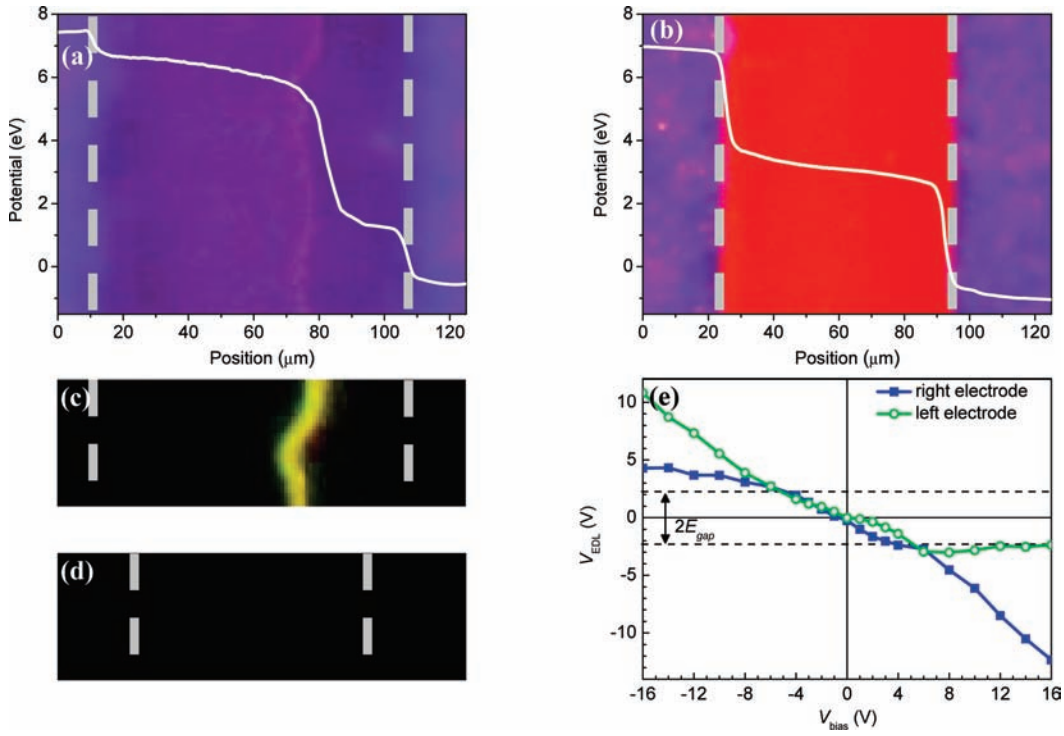

Figure 4. Electrostatic potential and light-emission profiles in planar LECs during operation and voltage dependence on the interfacial potential drop. Typical steady-state potential profiles of an LEC during operation at $V = 8$ V in (a), the noninjection-limited and (b), the injection-limited regime. The pictures behind the graphs are UV/PL images in steady state, on the same horizontal scale. Micrographs showing the presence or absence of light emission during steady-state operation at $V = 8$ V in (c), the noninjection-limited and (d), the injection-limited regime. The electrode interfaces are indicated by the white dashed lines in all micrographs. (e) Voltage-dependent potential drop over the interfacial regions for an injection-limited LEC. For positive bias voltages, the green line marked by open circles refers to the positive electrode.

p−n junction is dynamic. This behavior is evidently reproduced in our numerical modeling.

In order to substantiate the numerical results presented above, experiments were done on planar LECs by scanning Kelvin probe microscopy (SKPM) and electro-optical probing under UV-light. The former technique provides the electrostatic potential profile, whereas the latter indicates doping formation via doping-induced quenching of the UV-excited photoluminescence (PL), as well as a map of the light emission. The active layer comprised a conjugated polymer (either MDMO-PPV or SY-PPV), mixed with the salt KCF_3SO_3 and the ion-dissolving polymer PEO. The active layer is positioned amid two electrodes, defining an interelectrode gap of approximately 100 μm. Both types of measurement were performed on nominally identical devices under very similar, controlled circumstances. The fabrication of devices with and without injection limitations is described in the Experimental Section.

The experimental results are shown in Figure 4, with the electrode interfaces marked by vertical dashed lines. Figure 4a shows the steady-state potential profile of an LEC, with Au/Al top electrodes and SY-PPV as the conjugated polymer, that is not injection limited. The background shows the corresponding optical micrograph. Similar graphs have been obtained for MDMO-PPV-based active layers. In between the two electrodes, two doped regions, where PL is quenched, are visible, sandwiching a narrow junction region where light emission is observed (see Figure 4c). At the electrode interfaces potential drops of ~1.5 and ~1.0 eV are observed, indicating the presence of EDLs. In contrast to previous results on similar devices,[19] the potential drop over the EDLs is visible in our SKPM measurements. This is attributed to the use of an Al capping layer on top of the Au layer, which blocks the diffusion of ion-containing material through the electrode.[18] Note that equal electrodes are used, so that in order to form ohmic contacts the sum of the potential drops over both EDLs should be approximately equal to the bandgap of SY-PPV, i.e. 2.4 eV.[27] This is indeed the case. In the doped regions the potential is more or less constant, whereas a large potential drop is observed in a narrow region in the bulk: the light-emitting p−n junction. This behavior is fully consistent with the above calculations for a noninjection-limited device in the ECD limit (see black line marked by open circles in Figure 2). The final steady-state current through this device during operation was ~1.5 μA. The time dependence of the current will be discussed below.

Injection limitation was achieved by using Al electrodes that were allowed to oxidize slightly. Figure 4b shows the steady-state potential profile of an LEC with Al electrodes that shows all the attributes of being injection limited, as indicated by the large EDLs and the low electric field throughout the entire bulk. Furthermore, no significant doping was observed, as concluded from the absence of PL quenching in the optical micrograph, in line with the ED model. No light emission was observed during operation as shown in Figure 4d. The final steady-state current measured through this device was ~0.2 nA, being 4 orders of magnitude smaller than the current through the device operating in the noninjection-limited regime. Hence, the recombination rate and the light-emission intensity will be reduced by a similar factor, beyond the detection limit of the measurement system.

These experimental observations are in very good agreement with the numerical results for an injection-limited LEC (see

(27) Tseng, S. R.; Chen, Y. S.; Meng, H. F.; Lai, H. C.; Yeh, C. H.; Horng, S. F.; Liao, H. H.; Hsu, C. S. *Synth. Met.* **2009**, *159*, 137–141.

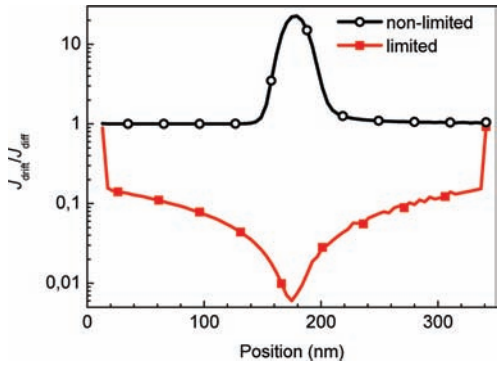

Figure 5. Drift-diffusion current ratio profile in simulated LEC devices in steady state. The profile of the device that has (no) injection limitation corresponds to the red (black) line with squares (circles).

red line marked by solid squares in Figures 2 and 3b). Note, however, that care should be taken not to confuse a noninjection-limited device with a p−n junction close to one of the electrodes with an injection-limited device, since both may have similar potential profiles. Therefore, the interfacial potential drop of the injection-limited LEC was determined as a function of bias voltage, see Figure 4e. The interfacial potential drop increases similarly at both electrodes for biases up to ±8 V. More important, at $||V_{bias}|| = 6$ V this potential drop surpasses the MDMO-PPV bandgap of ∼2.3 eV at *both* electrode interfaces. A p−n junction that has formed right next to an electrode in a noninjection-limited device can result in an interfacial potential drop larger than E_g. However, this cannot occur at both electrodes at the same time, as there can only be a single p−n junction in the device. Since the magnitude of the potential drop at a nonlimiting contact in the ECD is at most equal to E_g, the data in Figure 4e allow us to conclude that the device is truly injection limited and behaves according to the ED.

Another major difference between the ED and ECD is that the ED alleges the electronic bulk transport to diffusion rather than drift, since the ions screen the bulk from the external electric field. From the numerical results shown in Figure 2 and Figure 3, the ratio of the drift and diffusion contributions was determined, as shown in Figure 5. For the nonlimited case, the drift and diffusion contributions are equal in the doped regions. In the injection-limited case, diffusion dominates the total electronic current.

We will now rationalize these observations. First, consider only the ionic current. In steady state, the total ionic current must be zero, because of the ion-blocking electrodes and the absence of generation and recombination of ions. Thus, in the bulk, the drift and diffusion components of the ion current, $J_{i,drift}$ and $J_{i,diff}$, respectively, for both anions ($i = a$) and cations ($i = c$), must be equal but oppositely directed to obtain a zero total current: $J_{i,drift} = -J_{i,diff}$. A few steps are required to show that for a device in the ECD limit (i.e., a noninjection-limited device) this implies that $J_{p,drift} = J_{p,diff}$ holds for the hole current contributions in the p-doped region, and similar for electrons in the n-doped region. First, charge neutrality applies in the p-doped region, see Figure 3a, so hole and anion densities and their density gradients are equal. Second, holes experience the same electric field as anions. Therefore, the hole and anion drift currents, which are proportional to the product of density and field, are equal in magnitude, apart from a correction factor accounting for the difference in mobility. Also the hole and anion diffusion currents, proportional to the density gradient, are equal in magnitude, again apart from a correction factor accounting for the difference in diffusion constant. According to the Einstein relation the diffusion constant is proportional to the mobility; hence, both correction factors are identical, and $J_{p,drift} = J_{p,diff}$ follows from $J_{i,drift} = -J_{i,diff}$. The sign difference is due to the charge difference between holes and anions. A somewhat more elaborate derivation along these lines provides a general relation, valid for both injection-limited and noninjection-limited devices, between the electronic drift and diffusion currents at a position x in the doped region (see Supporting Information for a detailed derivation):

$$\left.\frac{J_{p,drift}}{J_{p,diff}}\right|_x = \tanh\left(\frac{q}{kT}(V(x) - V(x_1))\right) \quad (1)$$

for holes and

$$\left.\frac{J_{n,drift}}{J_{n,diff}}\right|_x = \tanh\left(-\frac{q}{kT}(V(x) - V(x_1))\right) \quad (2)$$

for electrons, with q the absolute electronic charge, k the Boltzmann constant, T the absolute temperature, V the electrostatic potential and x_1 the position of the center of the recombination zone. Since $\tanh(y)$ is in between −1 and 1 for any value of y, these relations limit the drift current in steady state to the diffusion current. The drift−diffusion current ratios in both injection regimes can now be identified. A large value of $(q)/(kT)(V(x) - V(x_1))$, e.g. due to the presence of a p−n junction, $q/kT \approx 40$ V^{-1} at 300 K, results in equal drift and diffusion currents. Without a junction, this value becomes smaller, effectively making the diffusion contribution dominant, cf. Figure 5.

During the simulations of both devices acting in different injection regimes, the current vs time and recombination rate vs time curves were also recorded as shown in Figure 6. Starting from $t = 0$, a large current is observed due to anions and cations moving in opposite directions. The electrodes block the ions, resulting in EDL formation, which reduces the field in the bulk, and hence the current goes down. After EDL formation, electrons and holes are injected and move through the active layer until they reach each other and recombine as denoted in Figure 6 with 1. The LEC in the injection-limited ED regime in Figure 6a shows a decreasing current after this point due to further screening of the electric field by increase of the EDLs. In contrast, the LEC in the noninjection-limited ECD regime in Figure 6b first shows a strong increase in current, which is electronic in nature and is due to doping formation in the bulk. This doping is then maximized, effectively reducing the electric field in the doped regions so that a p−n junction forms, as denoted by 2 in Figure 6b. After junction formation, the ions must adapt to the altered potential profile to reach steady state. Concomitant with this adaptation, the electronic drift current becomes limited to the diffusion current and thus decreases, as discussed at eqs 1 and 2. Because of this, a strong current drop after junction formation is observed in Figure 6b.

Comparison of the results of simulations and experiments in the insets of Figure 6 reveals that the characteristic features of the current transients are well reproduced by the model in both injection regimes. The quantitative differences in current densities and time scales can be attributed to the significantly different device lengths used, i.e. 350 nm in the simulations vs 100 μm in experiments, in combination with differences in applied bias and mobility values. Nonetheless, the similarity between the results from simulations and experiments convincingly consti-

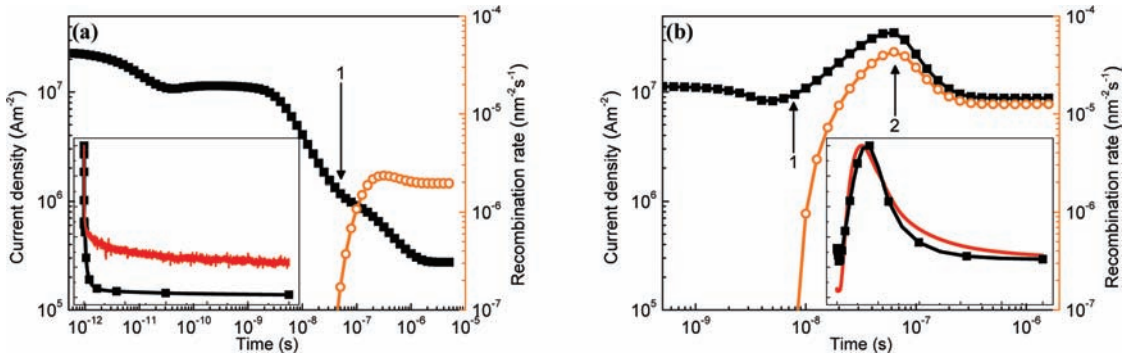

Figure 6. Transient current density and recombination rate in a simulated LEC device. Both devices started identically at $t = 0$ and were simulated until steady state was reached. The transient current density (black squares) and recombination rate (orange circles) for an injection-limited LEC (a) and a noninjection-limited LEC (b) are shown. The numbers 1 and 2 mark the initiation of recombination and junction formation, respectively. In the insets the calculated current density (black squares) is shown on a linear scale along with the experimental current trace (red). To enable comparison, horizontal and vertical axes have been normalized.

tutes the physical relevance of the numerical modeling results presented here.

Conclusions

Two operating regimes in LECs have been identified; their occurrence depends on the ability of the device to form noninjection-limited ohmic contacts. In the case where ohmic contacts are formed, the LEC follows the electrochemical doping model, characterized by the formation of a dynamic p−n junction in the bulk of the device. Anions and cations then become fully spatially separated across the junction at steady state, forming electric double layers at the contacts and doped regions in the bulk. In the case where injection of electronic charge carriers is limited, doping becomes less pronounced, and the ion redistribution increases the electric double layers until the bulk is screened from the external electric field. In this injection-limited regime, the device follows the electrodynamic model, and the electronic current is dominated by diffusion. In contrast, in the ohmic regime drift and diffusion contribute equally. Numerical studies as well as experiments confirm these findings.

These results imply that the electrochemical doping operation mode, i.e. without contact limitations, is the preferred operational mode for LECs, as it gives the highest current densities and the highest electron−hole recombination rates. They also imply that any degradation in the contact area, either by electrochemical side reactions[28,29] or by contact oxidation[30] may cause a transition to the electrodynamic operation mode and hence a reduction in current and light output. The often stated independence of LEC operation on contact material should thus be reconsidered.[31] Finally, our results show that the operational mode of an LEC-type device may be concluded from the shape of the current transient, and does not, per se, require elaborate SKPM experiments.

Acknowledgment. L.E. and P.M. acknowledge the Swedish Research Council (VR) and Wenner-Gren stiftelserna for scientific financial support. L.E. is a 'Royal Swedish Academy of Sciences Research Fellow' supported by a grant from the Knut and Alice Wallenberg Foundation.

Supporting Information Available: Derivation of eqs 1 and 2, implementation of injection models in numerical model, and additional numerical modeling results. This material is available free of charge via the Internet at http://pubs.acs.org.

JA1045555

(28) Fang, J.; Matyba, P.; Robinson, N. D.; Edman, L. *J. Am. Chem. Soc.* **2008**, *130*, 4562–4568.
(29) Johansson, T.; Mammo, W.; Andersson, M. R.; Inganas, O. *Chem. Mater.* **1999**, *11*, 3133–3139.
(30) Shin, J. H.; Matyba, P.; Robinson, N. D.; Edman, L. *Electrochim. Acta* **2007**, *52*, 6456–6462.
(31) Rodovsky, D. B.; Reid, O. G.; Pingree, L. S. C.; Ginger, D. S. *ACS Nano* **2010**, *4*, 2673–2680.